Pulsed Plasma Acceleration Modeling in Detonation and Deflagration Modes

IEPC-2019-A893

Presented at the 36th International Electric Propulsion Conference
University of Vienna – Vienna, Austria
September 15-20, 2019

Kurt A. Polzin[a] *and* Christine M. Greve[b]
NASA-George C. Marshall Space Flight Center, Huntsville, AL 35812, USA

Kamesh Sankaran[c]
Whitworth University, Spokane, WA 99251, USA

Gas-fed electromagnetic pulsed plasma accelerators discharge electrical energy into a gas to ionize and electromagnetically accelerate propellant in the domain. Efforts to model pulsed accelerators have either assumed that the discharge is short and completely transient, accelerating the gas by entraining it in a moving current sheet, or that the discharge is relatively long, establishing a stable quasi-steady current distribution pattern that accelerates a plasma flowing through it. There have been pulsed plasma accelerator tests that appear to fit somewhere between these two bounds, exhibiting some properties that are associated with the purely transient devices while also showing others that are associated with quasi-steady-state plasma acceleration. A model is presented based upon the premise that all pulsed plasma accelerators first form an accelerating current sheet (detonation mode accelerator). Depending upon the pulse length and the gas conditions in the discharge channel, the plasma sheet may reach the end of the accelerator before the discharge has completed a full half-cycle, wherein the proposed model transitions to a quasi-steady description of the acceleration process (deflagration mode accelerator). A review of the entire model is presented, highlighting improvements and upgrades implemented to aid in the stability of the numerical scheme used to model the gas flow in the channel and an improved treatment of current sheet mass shedding, which adds gas to the wake of the sheet. The assumptions employed to model the transition from detonation to deflagration mode are presented and used to generate solutions to the governing equations. The modeling of the deflagration-mode under the present assumptions results in very low deflagration impulse bits relative to those obtained at the end of the detonation mode, implying that the present assumptions and modeling of the deflagration mode may not represent a fruitful approach.

I. Introduction

Pulsed plasma accelerators for in-space propulsion applications apply an electrical pulse to an ionized gas, typically powered by energy stored in a capacitor or bank of capacitors. The resulting current pulse generates a magnetic field that interacts with the current to accelerate the gas through a Lorentz body force. The present work extends our previous modeling,[1,2] which has been aimed at studying the performance trends in two specific types of pulsed plasma accelerators: the gas-fed pulsed plasma thruster (PPT)[3] and the quasi-steady magnetoplasmadynamic (MPD) accelerator.[4]

A gas-fed PPT is typically understood and modeled as a transient accelerator in which the current pulse produces a current sheet at the breach of the accelerator.[5] That current sheet accelerates along the discharge

[a]Space Systems Team Lead, Advanced Concepts Office, kurt.a.polzin@nasa.gov.
[b]Presently: Graduate Research Assistant, Aerospace Engineering Department, Texas A&M University.
[c]Professor, Engineering & Physics Department.

channel under the action of a Lorentz body force, acting to maximize the inductance of the driving circuit while ionizing and entraining, or 'snowplowing', any gas the sheet encounters. This process typically occurs on the ∼1-10 μs timescale, producing a transient current pulse and a commensurate gas acceleration profile. The current sheet snowplowing into and entraining a neutral gas in the channel is analogous to a strong shock or 'detonation' wave in gas dynamics and combustion physics, and it is typically modeled using a one-dimensional momentum equation coupled to a set of circuit equations. Acceleration is typically considered to be completed once the current sheet reaches the end of the channel or the discharge current crosses zero, whereupon the current reverses and a new current sheet forms at the breach, depriving the existing plasma of additional energy for acceleration. The efficiency of such accelerators, defined as the ratio of jet kinetic energy to input electrical energy, is typically in the teens or lower.[6]

An MPD is typically understood as a steady-state device where the discharge current distributes throughout the channel, resulting in a more gradual electromagnetic acceleration of an ionized gas as it passes through the current channel. In this instance, the current channel is stationary and the gas passes through the distributed discharge in a manner similar to a 'deflagration' wave in gas dynamics and combustion. The MPD can further be said to operate in a quasi-steady mode, where the discharge is pulsed on the order of ∼1 ms or longer. In this mode, after a short initial transient period, the current and plasma conditions within the channel reach an approximate steady-state condition for most of the discharge pulse.[5] MPD thrusters can have high thrust densities and efficiencies approaching 50% for certain propellants and discharge power levels.[4]

While both the gas-fed PPT and the quasi-steady MPD thruster are generally well understood in terms of performance scaling, there are pulsed plasma accelerators that do not fit particularly well into this dual classification scheme. One of those devices is the Coaxial High ENerGy (CHENG) thruster.[7] This thruster operates on the PPT timescale of ∼10 μs, but claims efficiencies closer to those expected for an MPD thruster. Some PPT data also exhibit an odd scaling as a function of the amount of propellant injected per pulse (mass bit).[6,8] For most of the operating envelope, these particular gas-fed PPTs possess a low, constant efficiency as a function of mass bit (termed Mode I in that work), which aligns with the traditional expectations for a PPT. However, below some critical mass bit value the thruster efficiency increases with decreasing mass bit (termed Mode II in that work).

There are several studies in literature detailing investigations into these phenomena and classification-defying cases. A recurring explanation of these performance anomalies involves the use of a MHD formulation of the Rankine-Hugoniot model for detonation and deflagration waves with electrical energy addition taking the place of a combustion process.[7,9–11] A separate explanation examined the effects of plasma resistivity, which controls magnetic diffusion in the discharge channel.[12,13] In those works a low plasma resistivity was proposed to be characteristic of a propagating current sheet (detonation mode) while a highly-resistive plasma would allow the discharge to fill the volume faster and form a stationary plasma discharge (deflagration mode). Building off those studies, more recent work has studied the impact of the accelerator plume on a stationary target to gain insight into the acceleration process.[14,15] Using a resistive MHD model and downstream Schlieren imaging, this work attempted to describe the discharge as a sequence of events, with the controlling parameter being the delay between the start of gas injection and the initiation of the discharge. For a short delay, it was concluded that a high velocity deflagration jet would initially form, with a detonation wave forming in the gas that remained after the first half cycle of the oscillating discharge was completed. In the case of a longer delay, the data appeared to indicate that the resistivity was low enough to support the immediate formation of a detonation wave during the first half-cycle of the discharge.

Our work is similar to the more recent studies in that we focus on the discharge occurring as a sequence of events that occur over in a certain order. The view taken in the present paper is inspired by historical observations on the transition from the PPT mode of operation to a quasi-steady MPD mode. The discovery of the quasi-steady MPD mode occurred as researchers at Princeton extended the pulse length in PPTs through the use of pulse-forming networks. For pulse lengths longer than a certain geometry-dependent threshold value, the transient plasma current sheet transitioned to a diffuse MPD arc discharge that 'replicates in every observable detail steady flow self-field magnetoplasmadynamic acceleration.'[16] In addition, a propagating arc discharge was always observed in these experiments, suggesting that the acceleration process transitioned from detonation to deflagration mode as the pulse was extended.

We note two other items regarding the work in which the PPT Mode I/Mode II performance scalings were discovered.[6] First, the pulses in those thrusters did not ring, so there was no second half-cycle discharge. While the thruster operated with a pulse train consisting of several discharges closely spaced in time, the

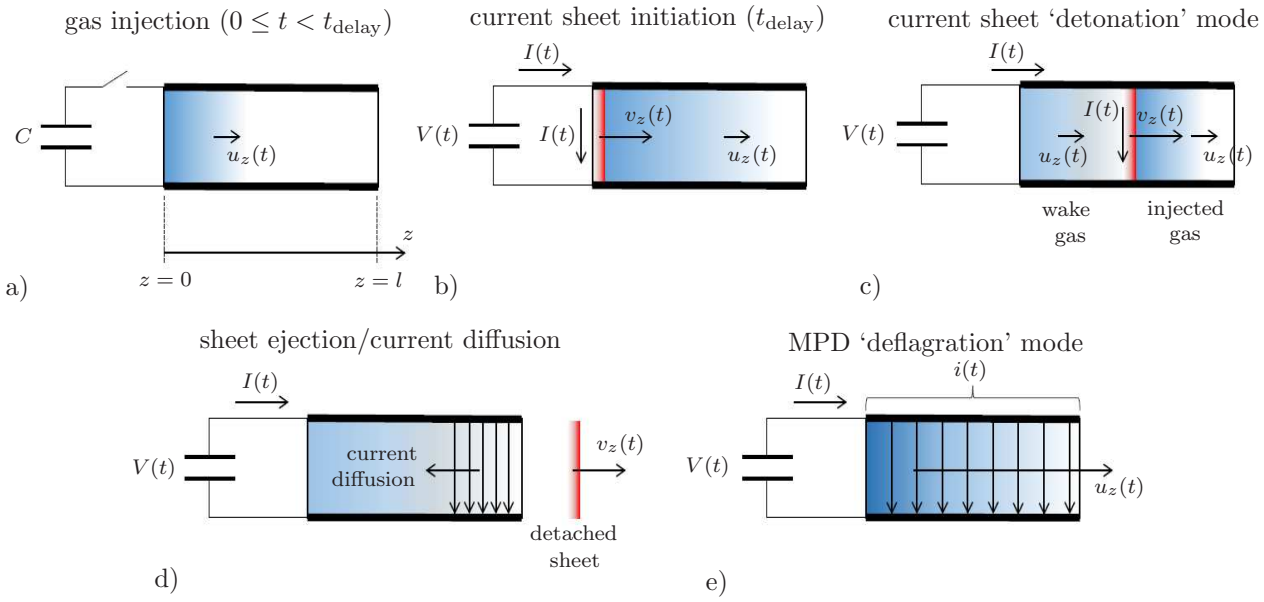

Figure 1. Proposed sequence of events in a pulsed plasma accelerator. a) Gas is injected for time $0 \leq t < t_{\text{delay}}$, b) the switch is closed and the current sheet forms at the accelerator breach at time t_{delay}, c) the current sheet snowplows into the gas ahead of it entraining some and leaving a wake of lower density gas (detonation mode), d) the current sheet exits the domain and the formerly-concentrated current rapidly diffuses back into the domain, and e) the distributed current pattern (deflagration mode) electromagnetically accelerates the gas left behind by the current sheet and any additional gas injected into the domain after the pulse was initiated.

discharge events were roughly 5 μs in length while the time between pulses was several hundred ms, which should have been a sufficient time for excess charge to have recombined to leave a neutral gas background for subsequent pulses. Second, there was a distinct pattern in the variation of the term

$$\int I^2 \, dt$$

as a function of mass bit for both Mode I and Mode II operation, strongly implying that the mass loading had an effect on the nature of the discharge current waveform. This integral is generally important in electromagnetic accelerators because it is indicative of the overall impulse imparted to the gas over the course of the discharge.

In the present work, we postulate the following sequence of events as a guide for our modeling work. Gas is first injected into the domain at time t=0 (Fig. 1a). At some time t_{delay} after t=0, the discharge is initiated in the channel. This controls the timing between gas injection and discharge initiation. In all cases, the discharge will collapse to the breach of the accelerator to yield a circuit with minimal initial inductance by forming a concentrated current sheet (Fig. 1b). The current sheet advances through any gas in the channel, entraining some fraction of the gas it encounters (Fig. 1c). Upon reaching the exit of the channel, the plasma in the current sheet is ejected out of the thruster at the speed it had attained, and through magnetic diffusion the current resistively diffuses backwards into the channel, filling it (Fig. 1d). This establishes the traditional quasi-steady MPD current pattern in the channel, which accelerates gas passing through the channel by a Lorentz body force (Fig. 1e). While we will not consider oscillations beyond the first half-cycle, it is straightforward to incorporate them into this model by simply returning to the step illustrated in Fig. 1b when the current reverses direction.

The outline for the rest of this paper is as follows. In section II we describe the model for the sequence of steps outlined in the previous paragraph. We then discuss the mechanics involved in actually generating a solution using the model in section III. A brief review of some of the important trends and results from past studies is presented in section IV and a set of solutions to the coupled detonation-deflagration mode problem for a certain set of conditions is found in section V.

II. Model

We proceed with a step-by-step description of the governing equations used to model a pulsed plasma accelerated by the Lorentz body force. We first provide the parameters of the accelerator under study in the present paper. The equations can be split into those governing fluid gas flow in the channel, those modeling an accelerating current sheet moving through the channel entraining gas (detonation mode), and those describing the acceleration of the gas as the current pattern organizes into a quasi-steady MPD configuration (deflagration mode).

Different time scales are required to solve the fluid and plasma sheet equations due to the differences in speed between the two objects of interest. The fluid is solved in an Eulerian frame of reference that is overlaid by a pulsed plasma thruster current sheet moving in a Lagrangian reference frame.

A. Thruster Properties

The present work assumes a pulsed plasma thruster possessing the properties shown in Table 1. The values in the table generally correspond to the coaxial accelerator studied in Ref. [10]. Major controllable variables in the simulation include the initial charge voltage, gas injection speed and density, and the timing between when gas in introduced into the channel and when the discharge current pulse is initiated.

Table 1. Properties for the Thruster Simulation

Thruster Length	23 cm
Inner electrode diameter	5 mm
Outer electrode diameter	5 cm
Capacitance C	112 μF
Stray inductance L_0	50 nH
Stray resistance R_e	5 mΩ
'Detonation' plasma resistance $R_{\mathrm{p,deton}}$	2.5 mΩ
Initial charge voltage	1000 V
Inlet gas temperature	298 K

B. Fluid Flow

The general conservation equations governing the evolution of a species of a fluid are given as

$$\frac{\partial \rho}{\partial t} + \nabla \cdot (\rho \mathbf{u}) = 0 \tag{1a}$$

$$\frac{\partial (\rho \mathbf{u})}{\partial t} + \nabla \cdot \left(\rho \mathbf{u}\mathbf{u} + \bar{\bar{P}} \right) = \nabla \cdot \bar{\bar{\tau}}_{\mathrm{vis}} + \mathbf{f}_{\mathrm{ext}} \tag{1b}$$

$$\frac{P}{\rho^{\gamma}} = \text{constant} \tag{1c}$$

where $\bar{\bar{P}}$ is the pressure tensor possessing a scalar value of P, $\bar{\bar{\tau}}_{\mathrm{vis}}$ denotes the viscous stress tensor, $\mathbf{f}_{ext}$ is an external body force applied to the control volume, and γ is the ratio of specific heats. These three equations represent, respectively, the conservation of mass density, conservation of momentum density, and an isentropic "closure" approximation used to solve for the evolution of the pressure within the domain.

Typically, viscous effects can be ignored in these types of problems. In the present work, we simplify the mass and momentum density equations to only describe flow in one dimension along the z-axis of the thruster (axial direction):

$$\frac{\partial \rho}{\partial t} + \frac{\partial}{\partial z}\left(\rho u_z\right) = 0, \tag{2a}$$

$$\frac{\partial \left(\rho u_z\right)}{\partial t} + \frac{\partial}{\partial z}\left(\rho u_z^2 + P\right) = \left(f_z\right)_{\text{ext}}, \tag{2b}$$

$$\frac{P}{\rho^\gamma} = \text{constant}. \tag{2c}$$

These equations are solved for every cell in the finite element domain to calculate the evolution of the mass and momentum density and the gas pressure injected into the channel. The solver includes a single ghost cell at the inlet and outlet of the channel. The inlet ghost cell is used to set a mass flowrate into the domain (which can be varied as a function of time) while the outlet ghost cell has a zero-gradient (Neumann) condition. The values for density, momentum, and pressure are stored at cell centers, so linear interpolation is employed to determine the values of these properties at cell interfaces.

In our model, the accelerating plasma sheet of the next section will entrain some percentage of the relatively slow-moving gas it encounters and 'shed' mass into the current sheet wake. The gas shed by the current sheet is assumed to drop out of the current sheet and return to the fluid solution domain at the speed of the fluid in that location, which simply adds to the fluid mass density. Strictly speaking, the interaction with the current sheet represents a sink (current sheet entrainment) and a source (current sheet gas shedding) in the momentum density equation, but since the fluid and current sheet are solved on different timescales, fluid density on the finite-element grid is simply adjusted accordingly after interacting with the current sheet.

The present version of the fluid model improves the stability of the solution through the incorporation of a numerical dissipation scheme. The spatial differencing scheme used here updates the values of both mass and momentum density using the fluxes of these quantities in and out of each cell in the domain. To prevent numerical instabilities that arise due to the inherently unstable nature of central differencing for hyperbolic (convection) problems, we introduce numerical diffusion in the scheme. A general diffusion term may have the form

$$Dz_{j+\frac{1}{2}} = \frac{1}{2}\left|\lambda_{\max}\right| \triangle U_{j+\frac{1}{2}} \tag{3}$$

where Dz is the diffusion for the $j+1/2$ boundary, $\lambda_{\max}$ is the largest eigenvalue of the system $(u_{\max}+c_s)$, and $\triangle U$ is the change in the value of a conserved quantity (mass density or momentum density) across that boundary. This diffusion term is subtracted from the original flux through the boundary of a cell and represents a low computational cost method to handle the instabilities of a central differencing scheme.[17,18]

C. Plasma Sheet Acceleration

The current sheet (detonation mode) is represented by a set of circuit equations coupled to a one-dimensional momentum equation. The model in this paper is written for a simple *RLC*-circuit, but it is a simple exercise to update this model to accommodate other pulsed electrical sources, such as pulse forming networks.

The set of equations governing the current dynamics is written as:

$$\frac{dV}{dt} = -\frac{I}{C}, \tag{4a}$$

$$\frac{dI}{dt} = \frac{V - I\left[\left(R_e + R_{\text{p,deton}}\right) + L_1 v_z\right]}{\left(L_0 + L_1 z\right)}, \tag{4b}$$

$$\frac{dz}{dt} = v_z, \tag{4c}$$

$$\frac{dv_z}{dt} = \left(\frac{L_1 I^2}{2} - {v_z}^2 \lambda_e A \rho\left(z\right)\right)/m, \tag{4d}$$

$$\frac{dm}{dt} = \lambda_e v_z A \rho\left(z\right) - \nu_L m. \tag{4e}$$

where L_1 is the inductance per unit length of the accelerator channel, A is the cross-sectional area of the channel, and $\rho(z)$ is the density of neutral gas encountered by the current sheet, given by the solution to

equation (2a). Equations (4a) and (4b) govern the discharge voltage V and current I, respectively, in an electrical circuit possessing an inductive element moving with an axial velocity v_z. The current sheet position z, velocity v_z, and mass m are modeled through equations (4c), (4d), and (4e), respectively.

The change in mass of the plasma sheet in equation (4e) was written differently in Ref. [2]. That paper was incorrect in the treatment of this equation, which is broken into two separate terms on the right hand side. The first term represents the mass entrained by the current sheet as it snowplows into a region of the domain. The user-controlled parameter λ_e is the entrainment efficiency, and it is used to adjust the amount of neutral gas that is entrained within the current sheet. A value of $\lambda_e = 1$ will result in full gas entrainment, while decreasing the value of λ_e will permit more of the encountered gas to pass through the current sheet without interaction.

The second term on the right hand side of equation (4e) reflects the mass lost by the current sheet. The lost mass reappears in the fluid domain once it has been shed by the current sheet. The term ν_L is a user-controlled parameter and is defined as the percentage of mass lost from the current sheet over a characteristic time interval. As an example, the value of ν_L for 10% current sheet mass loss in a microsecond would be $0.10/(10^{-6}$ s).

D. Current Sheet Wake

While solving the motion of the plasma current sheet, the motion of the gas in the wake behind the current sheet must also be considered. Once the plasma sheet passes a location, mass may be left behind it, either because the encountered gas was not entrained ($\lambda_e < 1$) or because the current sheet has 'shed' some amount of its previously-entrained mass ($\nu_L > 0$). Note that it may require several current sheet solution timesteps before the sheet crosses a fluid cell, and the mass shed from the sheet into the cell is the aggregate of all the mass losses for each time step during this transit.

The net gas in the wake is represented by the sum of gas that was not entrained or was shed from the current sheet, and this gas is assumed to have the same velocity as the gas that was in the cell prior to encountering the current sheet. The wake mass density and velocity are then used to calculate a momentum density and pressure in the cell, which can be used to further advance the wake fluid in time using the governing set of equations (2). The generation of the data set representing the wake fluid only occurs while the current sheet is propagating through the domain. Once the current sheet exits the domain, the model for the electrical pulse and the acceleration of the working fluid transitions to the deflagration mode.

E. Stationary Plasma Model

If the electrical pulse has not completed a full half-cycle of the discharge before the plasma sheet reaches the end of the domain, then the model transitions to the deflagration mode of acceleration. In physical terms, detonation-mode acceleration involves a highly-conductive plasma where all the current is concentrated in the advancing current sheet. Once this sheet reaches the end of the domain, we consider, for the purposes of this model, that the current sheet detaches from the electrodes and leaves behind a very weakly-ionized, highly-resistive gas in the channel. The process of current detaching from the electrodes is much more complex than what is considered here. The approximation considered in this study is used for the purposes of simplifying the model to a point where it can be used to generate insight into the overall process.

If the electrical pulse has not completed a full half-cycle, then once the current sheet decouples and detaches there is still voltage on the capacitor bank driving the discharge. There is also the removal of the voltage drop across the channel owing to the loss of the IdL/dt term in equation (4b) [$IL_1 v_z$]. Current continuity must still be maintained, however, implying that the circuit resistance presented by the plasma will grow significantly after the current sheet detaches, which is in-line with the current sheet leaving a highly-resistive plasma in its wake.

The high value of electrical resistivity of the channel will result in a significant amount of resistive diffusion of the current density ($\mathbf{j}$ in A/m^2), which will reorganize itself and quickly spread backwards from the end of the channel towards the breach of the thruster. This process can be described using the classical diffusion equation,

$$\frac{\partial \mathbf{j}}{\partial t} = \nabla \cdot \left(\frac{\eta}{\mu_0} \nabla \mathbf{j} \right) \simeq \frac{\eta}{\mu_0} \nabla^2 \mathbf{j}, \tag{5}$$

where $\mathbf{j}$ is the current density vector, η is the resistivity of the gas, and μ_0 is the magnetic permeability of free space. The diffusion process results in the current channel expanding over time to a width of,

$$\delta(t) = \sqrt{\frac{\eta\, t}{\mu_0}}. \tag{6}$$

We can approximate the variation in resistivity as a function of temperature as $\eta \propto T^{-3/2}$. For our model, under the adiabatic assumption employed for equation (2c) and further employing an ideal gas equation of state, it is straightforward to show that the resistivity scales inversely with density.

If the resistivity of the upstream plasma is $\eta \simeq 1$ Ω-m, then the timescale for the diffused current to fill the length of the channel $\delta \simeq l \simeq 0.1$ m is approximately $\tau_{\text{diff}} \simeq 10$ ns. This is much faster than every other process in the post-detonation mode problem, making it reasonable to treat the current as having reached a diffusive equilibrium, being equally distributed throughout the channel during the deflagration mode.

The stationary current pattern established through resistive diffusion imparts electromagnetic acceleration to the plasma that moves through it, accelerating the fluid out of the channel. In this mode, because the stationary plasma does not have a time-varying inductance or plasma sheet motion, the resulting equations governing the behavior of the circuit become

$$\frac{dV}{dt} = -\frac{I}{C}, \tag{7a}$$

$$\frac{dI}{dt} = \frac{V - I\,(R_e + R_{\text{p,deflag}})}{(L_0 + L_1 l)}, \tag{7b}$$

where l is the length of the accelerator. The end values for the capacitor voltage and current obtained from equations (4a) and (4b), evaluated when the current sheet exits the domain, represent the initial values for the solution of equations (7a) and (7b).

In the detonation mode, the power deposited from the primary circuit into plasma acceleration is represented as $I^2 dL/dt$. In the stationary deflagration mode the inductance does not vary as a function of time, so to maintain continuity of the discharge current after plasma sheet detachment we increase the power transfer to the plasma in our model using an enhanced resistance. As we do not have a detailed plasma model and are only treating the plasma as a one-dimensional fluid, we approximate the value of the enhanced resistance for the deflagration mode (deflag) using the circuit values from the end of the detonation mode (deton) to obtain

$$\begin{aligned} R_{\text{p,deflag}} &= R_{\text{p,deton}} + \left.\frac{dL}{dt}\right|_{\text{sheet ejection}}, \\ &= R_{\text{p,deton}} + L_1 v_z|_{\text{sheet ejection}}\,. \end{aligned}$$

For the present work, this value is taken as a constant for the duration of the deflagration mode, which is an approximation that has the effect of decoupling the electrical circuit response from the plasma acceleration process. This allows the former to be solved completely before calculating the deflagration mode electromagnetic acceleration imparted to the gas. Equations (7) are solved until the current reaches a zero-value. If the value of $R_{\text{p,deflag}}$ pushes the circuit into an overdamped oscillatory response, then we cease the calculation when the current value is 10% of the peak current in the simulation. Below this level, the contribution to the overall impulse bit is small.

The solution for the discharge current is used to calculate the electromagnetic body force on the fluid. The electromagnetic force applied to the fluid in one cell of the domain is equal to,

$$(F_z)_{\text{ext}}(t) = \frac{L_1\, i(t)^2}{2}. \tag{8}$$

where i is the total current in one cell of the fluid domain (equal to $I(t)$ divided by the number of cells for a constant cell size). This force can be converted to a body force (force per unit volume) for each cell by dividing by the differential size of the cell ($A\,\Delta z$) to yield

$$(f_z)_{\text{ext}}(t) = \frac{L_1\, i(t)^2}{2\, A\, \Delta z}. \tag{9}$$

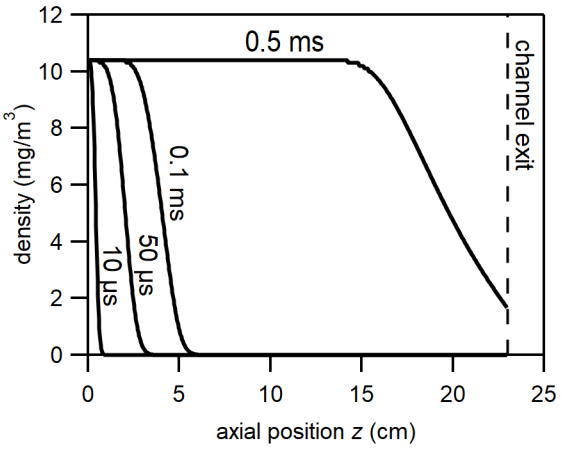

Figure 2. Neutral gas density in the channel at different instances of time for a mass flow rate of 8 mg/s.

This external body force term is calculated using values of the current waveform interpolated to the time for each fluid time step. The fluid equations are exactly those described by equations (2), with this body force term used in equation (2b). Since the electromagnetic term is dominant in the deflagration mode, we neglect the contribution of pressure in computing these solutions (also, the electromagnetic addition of energy makes the gas acceleration a non-isentropic process).

III. Generating Solutions

In this section we describe the mechanics involved in using the models of the previous section to generate solutions.

The solution begins with an empty domain. The injection ghost cell at the left-hand side of the domain uses a user-defined mass flow rate and pressure with a calculated thermal velocity to inject gas into the domain. The neutral gas history is found by first discretizing equations (2) in time and space and then solving them for every cell in the domain as the code advances through time. As gas continues to be injected into the domain, the gas front begins to elongate in the direction of the channel exit. Figure 2 depicts gas density in the domain calculated for different injection times, showing the elongation of the front as it expands towards the vacuum exit.

The plasma current sheet is initiated at a time t_{delay} that is specified by the user. The gas load in the channel before the discharge is initiated is completely under the control of the user, who can adjust both t_{delay} and the mass flow rate.

Once the plasma sheet is initiated, two solvers are operating in parallel, each with its own time step. The solver for the fast plasma sheet described by equations (4) and moving in a Lagrangian reference frame completes multiple smaller time steps relative to the fluid solver, which advances the solution to equations (2) at roughly the thermal speed of the gas moving in an Eulerian reference frame. The latter must not only solve the continuing temporal evolution of the gas ahead of the current sheet, but it must also advance a solution to the gas remaining in the current sheet wake. The most difficult part of this process is accounting for the current sheet mass entrainment and gas shedding processes, which demands a transfer of mass between the two solvers.

After the plasma sheet solution advances through one fluid solver time step, the solution to the former is halted, with the conditions in the plasma sheet at this point used as the initial conditions for the next fluid time step. During each fluid solver time step, the gas ahead of the current sheet is evolved in time. Mass that was not entrained by the plasma sheet and the mass shed by the plasma sheet are calculated using the terms of equation (4e). These mass components comprise the fluid wake of the plasma sheet.

The solution of the plasma sheet rapidly advancing into the slower-moving gas ahead of it can be solved independent of a wake solution since the fluid wake does not affect the plasma sheet or gas ahead of it. Once the solution of the plasma sheet and the gas ahead is generated to the point where the sheet leaves

the domain, we then generate the wake gas data set. The set must be generated behind the plasma sheet as it moves across each fluid cell, and the set must be advanced in time on the fluid timescale while it is being generated. The contributions to each finite element cell are summed over the time it takes for a sheet to cross that cell to generate total values for each cell as a cell-centered value. Special care is taken to make sure that the time elapsed from the initiation of the plasma sheet to it reaching the end of the channel is equal to the time taken to generate the wake fluid data set. While this is happening, gas injection at the inlet can also still be occurring, supplementing the wake fluid.

The value of the discharge current is checked when the plasma sheet reaches the end of the thruster channel. If the current has not crossed zero, meaning that the electrical pulse has not completed a half-cycle, then it transitions to a deflagration mode accelerator model. The plasma sheet detaches from the electrodes and the current in the domain is assumed to rapidly diffuse back towards the breach until a diffusive equilibrium is reached where the current density distribution in the channel is constant. This occurs in such a short period of time that the domain in the deflagration mode is simply considered to immediately be in this equilibrium state once the plasma sheet detaches.

In the deflagration mode, the voltage and current waveforms are generated using equations (7a) and (7b). Using our approximation for $R_{\mathrm{p,deflag}}$ makes these equations independent of the plasma acceleration process. This allows us to solve the current evolution in its entirety to the point of current reversal before returning to the fluid solver to calculate the plasma acceleration in the deflagration mode.

The acceleration of the gas in the channel is calculated for the time between when the plasma sheet detaches and when the discharge current reverses. The fluid equations (2) are advanced in time on a longer time step than the solution for the discharge current. The external electromagnetic force on the plasma in the channel is calculated using equation (9) with the current waveform found previously.

The impulse per pulse or impulse bit I_{bit} imparted to the fluid is calculated as the sum of three contributions, which are given in Table 2.

Table 2. Various components comprising the total impulse bit of a pulsed thruster

contributor to I_{bit}	amount of contribution	location/time of evaluation
plasma sheet	$m_{\mathrm{sheet}} v_z$	evaluated at detachment
exit gas flux	$\int \dot{m} u_z \, dt$	at the exit
gas in channel after pulse	$\int \rho u_z \, A \, dz$	entire domain

Once the impulse bit in computed, the thruster efficiency η_{t} can be found as

$$\eta_{\mathrm{t}} = \frac{I_{\mathrm{bit}}^2}{2 m_{\mathrm{bit}} E},$$

where m_{bit} is the total mass injected into the domain for the entire simulation and E is the discharge energy, equal to $CV_0^2/2$, where V_0 is the initial charge voltage on the capacitor bank.

IV. Review of Previous Solutions

In previous work,[1,2] we studied the initial gas injection into the domain along with the detonation mode and quantified the effects of changing model parameters such as the mass flow rate, mass entrainment coefficient λ_e, the plasma sheet initiation time t_{delay}, and the mass loss coefficient ν_L. We proceed with a short review of the trends that were observed in those studies, specifically focusing on the state of the solution at the end of the detonation mode since that represents the initial state for the deflagration mode plasma solutions.

The gas density in the channel evolves as a function of time in the manner illustrated in Fig. 2. The specific density numbers are for 8 mg/s, but the distribution always assumes this general form regardless of the flow rate with the expansion of the gas front occurring over approximately the same spatial distance. The particular simulation shown in the figure was used to determine the time it takes for the gas front to reach the end of the channel, which is 410 μs.

We performed a detonation mode simulation for an impermeable plasma sheet that entrained all the propellant it encountered ($\lambda_e = 1$). We found that as we repeated this simulation while lowering the value

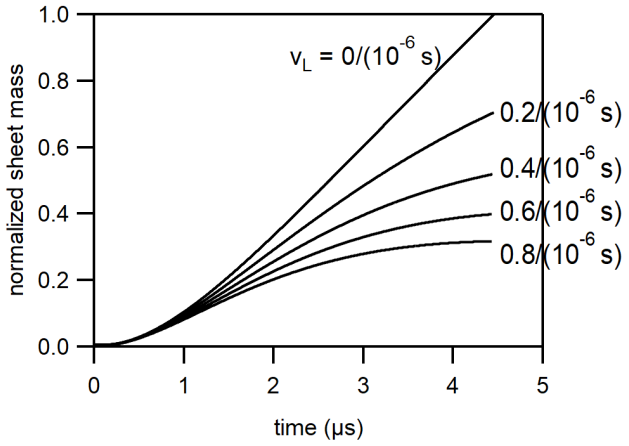

Figure 3. Normalized detonation-mode plasma sheet mass as a function of time for varying mass loss coefficients ν_L. The end time for each waveform represents the time that the sheet reached the end of the channel.

of λ_e, the time required for the plasma sheet to reach the end of the thruster was reduced. This trend is the result of two factors. One is a reduced drag resistance on the accelerating plasma sheet. The other is an increase in the sheet acceleration that occurs because the force is relatively unchanged early in the pulse but the mass being accelerated is greatly reduced. The sheet moving faster as λ_e is decreased also increases the value of $I \cdot dL/dt$ in the circuit equations, which serves to reduce the peak current level attained in the detonation mode, adding significant variation to the initial conditions for the deflagration mode solution.

We have not previously solved a set of problems using the definition of the mass loss coefficient ν_L given in this paper (percent of current sheet mass lost per μs). Data illustrating the effect this parameter has on the current sheet mass are presented in Fig. 3. These data are normalized such that the value 1 represents the mass at the end of the solution for $\nu_L = 0$. As expected, the terminal plasma sheet mass is reduced as the value of ν_L is increased. The mass loss coefficient has only a very minor effect on the acceleration of the plasma sheet, with all the waveforms reaching the end of the channel at approximately the same time. This, coupled with the observations on the effects of varying λ_e, seems to imply that the acceleration of the plasma is affected far more by drag resistance than by a reduction in the inertia of the sheet.

To verify mass conservation, we calculated the integrated neutral gas mass injected into the domain during a simulation and compared that to the sum of the mass entrained by the plasma sheet, the mass not entrained by the plasma sheet, and the mass shed by the plasma sheet. These terms agreed with the integrated gas injection mass, so mass is conserved in our numerically-generated solutions.

As a note on the interaction of plasma sheet mass entrainment and shed mass, one can imagine that there are certain combinations of the entrainment coefficient λ_e and mass loss coefficient ν_L that would result in the plasma sheet reaching an equilibrium mass where it entrained and shed the same amount of mass in each step size.

V. Full Problem Solutions

In past studies we have focused on generating solutions to limited portions of the problem. In the present section we proceed with the generation of a solution set that starts in the detonation mode and transitions into the deflagration mode.

For the present solution set we will vary only t_{delay} while keeping all other parameters constant. This will alter the amount of gas that has been injected into the channel before the discharge is initiated. The rate of gas injection is 8 mg/s, the value of λ_e is 0.6, and ν_L is set equal to $0.1/(10^{-6}$ s). The gas density distributions at the times of plasma sheet initiation are given in Fig. 2.

Solutions to the discharge current as a function of time are given in Fig. 4. This graph illustrates both the initial detonation-mode current waveforms (solid lines) and the subsequent deflagration mode waveforms (dashed lines). We observe that each current trace follows the same initial trend as the density of gas near

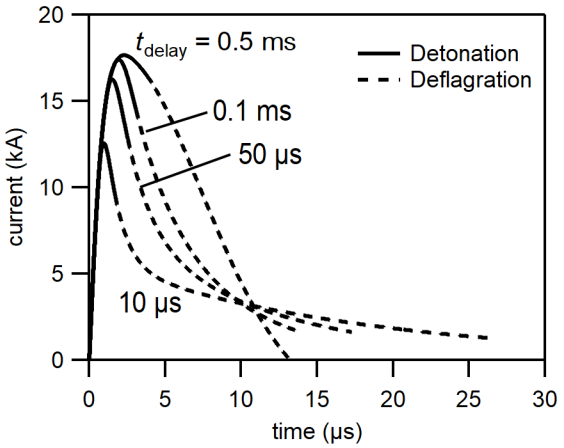

Figure 4. Discharge current waveforms for varying values of t_{delay}, showing the detonation (solid line) and deflagration (dashed line) portions of the discharge.

the breach of the thruster is the same in each case. However, as the sheets advance, they all enter a region of significantly lower density at some point in the domain. We would expect a current sheet to accelerate more rapidly in this region of lesser density, significantly limiting the peak current attained during the discharge for the reasons discussed in the previous section and as depicted in this figure. Note that because we do not have a detailed plasma or resistivity model, we are 'patching' the two solution modes together by assuming a deflagration mode plasma resistance. Sometimes this value pushes the solution into the overdamped regime and the current pulse never reaches a zero value. When this occurs, we consider the pulse complete when the current decreases to 10% of the peak current value.

Whenever the mass entrainment coefficient $\lambda_e < 1$ or the mass loss coefficient $\nu_{loss} > 0$, there will exist some gas in the wake of the plasma sheet. For ease of visualization and discussion, these two methods of fluid being left in the wake are plotted separately in Fig. 5, though they are combined into one wake fluid for calculations in the actual model. The gas that is not entrained by the plasma sheet is given as $(1 - \lambda_e)\rho(z)$. For our case where λ_e is 0.6, this results in density distributions in Fig. 5a that are roughly 40% of those found in Fig. 2, as desired. The rise in the gas density at the breach of the thruster is caused by additional gas that gets injected into the domain while the plasma sheet accelerates towards the channel exit. For these models, the gas injection is never stopped.

The mass shed by the plasma sheet, plotted in Fig. 5b, requires a more complex explanation. After a short transient stage at the start of the calculation where the initial mass of the plasma sheet informs the mass shed term for the first few cells, the net mass shed from the current sheet increases as the sheet moves in the axial direction. This is because the sheet mass in increasing as it encounters and entrains more propellant moving along the domain. The continued increase in plasma sheet mass is indicative of the mass entrainment term remaining larger than the mass loss term. However, once the sheet moves into a region where gas has not yet reached or is very sparse, the sheet mass is seen to decrease because it is no longer entraining enough mass to compensate for the mass that is shed. Near the channel exit the first few test cases are seen to be approaching a steady-state plasma sheet mass, meaning that the entrainment and mass loss terms are balancing in some form of equilibrium.

Using the input conditions presented in Figs. 4 and 5, we proceed with the solution of the deflagration mode, ending our computation when the first half-cycle of the current is complete. The final mass density and momentum density distributions of the gas in the discharge channel are given in Figs. 6a and 6b, respectively. For varying values of t_{delay}, the gas exhibits motion through the domain as it is fed by gas injection from the left-hand boundary and accelerated by the electromagnetic force provided by the current in a manner highly similar to the initial neutral gas injection. In Fig. 6b we see that the momentum curve labeled $t_{\text{delay}} = 0.5$ ms is separated somewhat from the other curves for the first 8 cm of axial distance. Referring back to Fig. 4, we observe that the current pulse for that case had the highest values in the detonation and deflagration mode. Since the electromagnetic force scales with I^2, it makes some sense that this set of data would exhibit

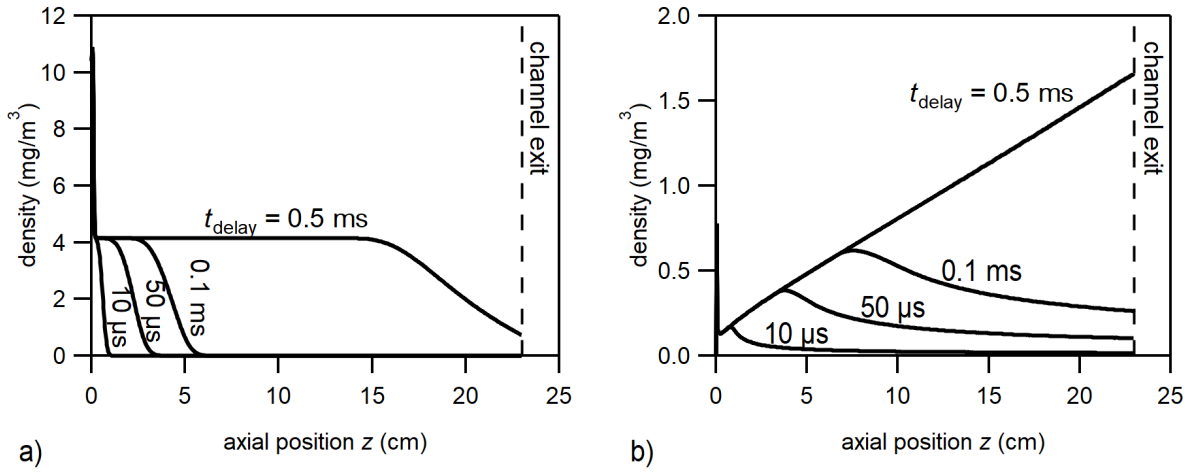

Figure 5. Gas density in the wake of the plasma sheet for the values of t_{delay} as indicated where a) represents gas that was not entrained by the plasma sheet (for λ_e of 0.6) and b) represents mass shed by the plasma sheet (for ν_L equal to $0.1/(10^{-6}$ s)).

some added momentum relative to the other cases. Also note that because the velocity of the wake gas as the plasma sheet traverses the domain remains the velocity from the neutral gas injection, the momentum terms are almost approximates of the mass density multiplied by a constant velocity, hence the similarity in plot shape.

Presented in Table 3 are the detonation and deflagration-mode contributions to the thruster I_{bit} computed under the assumptions of the present work. We observe that the detonation-mode impulse bit increases with increasing t_{delay}, which serves to more fully load the channel before initiation of the current discharge. What we do not yet see is a large contribution from the deflagration mode, though it appears to have an opposite trend than the detonation mode.

Table 3. Computed Detonation and Deflagration-mode contributions to the overall thruster impulse bit

t_{delay}	Detonation I_{bit} $(\mu N - s)$	Deflagration I_{bit} $(\mu N - s)$
10 μs	36.8	1.0
50 μs	91.9	0.30
0.1 ms	132	0.21
0.5 ms	179	0.15

It is important to note here that two assumptions made for the deflagration mode model may need to be revisited in future work to improve the deflagration model. The first assumption, the method of calculation of the plasma resistance, could be incorrect and artificially affecting the discharge current in an unintended manner. The second assumption is that the discharge current distributes evenly throughout the entire thruster channel in its equilibrium state regardless of the present gas in a given location. There is the possibility that the current distribution is directly affected by the presence of gas in that the current distribution may only exist where there is sufficient gas to support current conduction. This would concentrate the current in the actual regions where gas is present to allow for better acceleration of the wake gas.

VI. Conclusions

We have presented a one-dimensional model of gas-fed pulsed plasma accelerator operation centered around an external circuit coupled to a momentum equation. The model is based upon the hypothesis that these pulsed plasma devices operate through a series of distinct, discrete steps, starting as a pulsed plasma

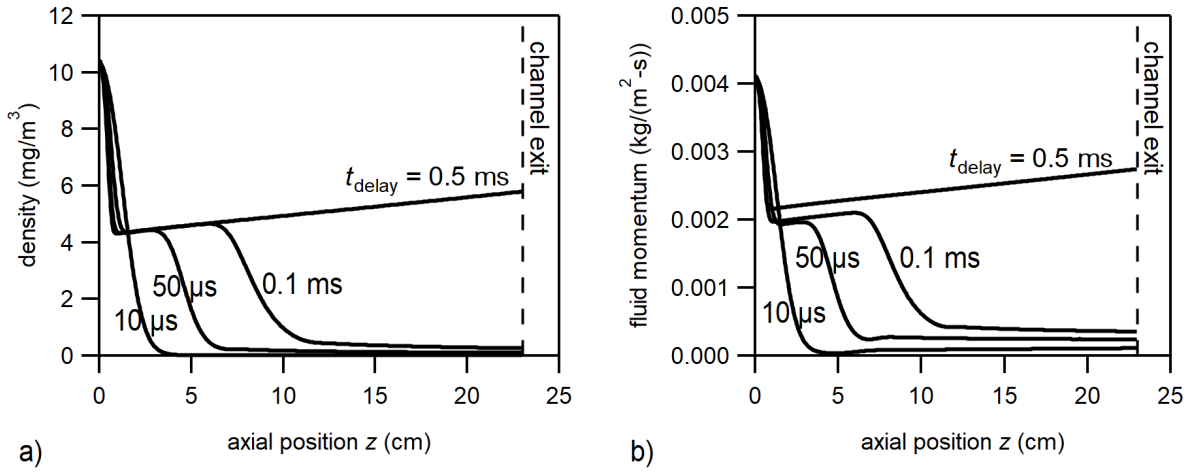

Figure 6. a) Gas density and b) momentum density distributions in the channel at the end of deflagration-mode acceleration.

thruster creating and accelerating a current sheet in a detonation mode of operation and then transitioning to a quasi-steady MPD deflagration mode upon the ejection of the current sheet. Enhancements to the previous model include the implementation of a numerical dissipation scheme in the fluid solver to increase stability and the implementation of a new way to handle mass shedding from the current sheet as it accelerates towards the exit of the thruster. As in past studies, we found that the current sheet reached the end of the channel faster when there was less mass to entrain, lowering the drag exerted on the current sheet and resulting in a reduction of the discharge peak current. As the current sheet exits the domain, the proposed model transitions from the detonation mode to the deflagration mode, operating in the latter until the current half-cycle is complete and the discharge current reverses itself.

Knowledge of the end-state of the detonation mode is important since that forms the basis for the initial conditions of the deflagration mode solution. Since we do not have a detailed plasma model from which we can calculate transport properties like plasma resistivity, we opt to invoke some assumptions regarding the nature of the deflagration mode circuit resistance and the distribution of current in the channel once the current sheet exits the channel. Specifically, we assumed that at the end of the detonation mode the current would re-distribute itself evenly along the length of the channel and that the resistance would increase such that the impedance at the beginning of the deflagration mode matched that at the end of the detonation mode. The impulse bit contribution of the detonation mode is in line with expectations, but the deflagration mode contribution is significantly lower than expected. We expect that the source of our issues lies with the transition to the deflagration mode since that process involves some very large approximations and assumptions. Future work will involve investigating those assumptions and alternatives that can be used in lieu of what is presented in this paper. However, it may be that this problem is beyond the scope of what can be captured with a one-dimensional circuit-based model.

Acknowledgments

The authors acknowledge several helpful discussions with A. Martin, J.B. Pearson, T. Moeller, M. La-Pointe, M. Glascock, and A. Ratcliffe, which have improved the quality of this work.

References

[1]K.A. Polzin and C.M. Greve, "Acceleration Modes and Transitions in Pulsed Plasma Accelerators," *AIAA Science and Technology (SciTech) Forum*, Kissimmee, FL, Jan. 8-12, 2018. AIAA Paper 2018-174.

[2]K.A. Polzin and C.M. Greve, "Modeling of Initial Detonation-mode Acceleration in Pulsed Plasma and Magnetoplasmadynamic Thrusters," *AIAA Propulsion and Energy Forum*, Cincinnati, OH, July 9-11, 2018. AIAA Paper 2018-4728.

[3]J. Marshall, "Performance of a Hydromagnetic Plasma Gun," *Phys. Fluids*, Vol. 3, No. 1, 134–135 (1960).

[4]R.L. Burton, K.E. Clark, and R.G. Jahn, "Measured performance of a multimegawatt MPD thruster," *J. Spacecraft Rockets*, Vol. 20, No. 3, 299–304 (1983).

[5]R.G. Jahn, *Physics of Electric Propulsion*, McGraw-Hill, New York, 1968.

[6]J.K. Ziemer, "Performance scaling of gas-fed pulsed plasma thrusters," *Ph.D. Dissertation*, Mechanical and Aerospace Engineering, Princeton Univ., Princeton, NJ (2001).

[7]D.Y. Cheng, "Plasma deflagration and the properties of a coaxial plasma deflagration gun," *Nucl. Fusion*, Vol. 10, 305–317 (1970).

[8]J.K. Ziemer and E.Y. Choueiri, "Scaling laws for electromagnetic pulsed plasma thrusters," *Plasma Sources Sci. Technol.*, Vol. 10, No. 3, 395–405 (2001).

[9]F.R. Poehlmann, N. Gascon, and M.A. Cappelli, "The Deflagration-Detonation Transition in Gas-Fed Pulsed Plasma Accelerators," *AIAA Joint Propulsion Conference*, Cincinnati, OH, July 8-11, 2007. AIAA Paper 2007-5263.

[10]F.R. Poehlmann, M.A. Cappelli, and G.B. Reiker, "Current distribution measurements inside an electromagnetic plasma gun operated in gas-puff mode," *Phys. Plasmas*, Vol. 17, 123508 (2010).

[11]F.R. Poehlmann, "Investigation of a Plasma Deflagration Gun and Magnetohydrodynamic Rankine-Hugoniot Model to support a Unifying Theory For Electromagnetic Plasma Guns," *Ph.D. Dissertation*, Dept. of Mechanical Engineering, Stanford Univ., Stanford, CA (2010).

[12]D.M. Woodall and L.K. Len, "Observation of current sheath transition from snowplow to deflagration," *J. Appl. Phys.*, Vol. 57, No. 3, 961–964 (1985).

[13]H. Sitaraman and L.L. Raja, "Magneto-hydrodynamics simulation study of deflagration mode in co-axial plasma accelerators," *Phys. Plasmas*, Vol. 21, 012104 (2014).

[14]V. Subramaniam and L.L. Raja, "Magnetohydrodynamic simulation study of plasma jets and plasma-surface contact plasma accelerators," *Phys. Plasmas*, Vol. 24, 062507 (2017).

[15]V. Subramaniam, T.C. Underwood, L.L. Raja, and M.A. Cappelli, "Computational and experimental investigation of plasma deflagration jets and detonation shocks in coaxial plasma accelerators," *Plasma Sources Sci. Tech.*, Vol. 27, No. 2 (2018).

[16]K.E. Clark and R.G. Jahn, "Quasi-steady plasma acceleration," *AIAA J.*, Vol. 8, No. 2 (1970).

[17]K. Sankaran, "Simulation of Plasma Flows in Self-Field Lorentz Force Accelerators," *Ph.D. Dissertation*, Mechanical and Aerospace Engineering, Princeton Univ., Princeton, NJ (2005).

[18]A. Jameson, "Analysis and Design of Numerical Schemes for Gas Dynamics, 1: Artificial Diffusion, Upwind Biasing, Limiters and Their Effect on Accuracy and Multigrid Convergence," *Comp. Fluid. Dyn.*, Vol. 4, 171–218 (1995).